Journal of Molecular Modeling (2019) 25: 254
https://doi.org/10.1007/s00894-019-4105-5

ORIGINAL PAPER

Ab initio study on the six lowest energy conformers of iso-octane: conformational stability, barriers to internal rotation, natural bond orbital and first-order hyperpolarizability analyses, UV and NMR predictions, spectral temperature sensitivity, and scaled vibrational assignment

Mouhi Eddine Hachim[1] · Karima Sadik[1] · Said Byadi[1] · Christian Van Alsenoy[2] · Aziz Aboulmouhajir[1,3]

Received: 6 June 2018 / Accepted: 26 June 2019 / Published online: 30 July 2019

Abstract

In this paper, we present the quantum electronic study of iso-octane, based on MP2 and B3LYP methods using the 6-311++G(d,p) basis set. In addition to conformational stability and internal rotation barriers studies, the delocalization energies associated with the internal charge transfer (ICT) within each of the six lowest energy conformers were evaluated using NBO analysis. With the aim to differentiate even more between these conformers, the energy gap between HOMO and LUMO orbitals, chemical softness, and first-order hyperpolarizability (nonlinear optics property) were evaluated. Similarly, their spectral behavior was investigated at different levels; the ultraviolet (UV) absorption bands were assigned using molecular orbitals data obtained by TD-B3LYP calculations with 6-311++G(d,p) basis set, while carbon ^{13}C NMR and proton ^{1}H signal peaks were assigned using the GIAO-B3LYP/6-311++G(d,p) method. In addition, the normal mode calculations of the most and least stable conformers using a scaled force field in terms of nonredundant local symmetry coordinates were carried out to approach the vibrational spectra temperature dependency.

Keywords Ab initio · Conformational isomerism · Natural bond orbital · First-order hyperpolarizability · UV absorption bands · ^{13}C and ^{1}H NMR spectra · Scaled vibrational analysis

Introduction

The branched hydrocarbon 2,2,4-trimethylpentane (TMP), often referred to iso-octane, commonly results in the processing of crude petrol and therefore is of great interest in the petrochemical industry [1]. Moreover, turbocharging causes excessive detonation, accompanied by an extreme rise of temperature and pressure in the combustion chamber leading to the knocking noise [2]. Because the latter is very damaging for both human and equipment, the use of gasolines with an antiknock value, i.e., the ability to withstand the compression, has proven vital. This ability is measured by the octane number as an indicator of energy efficiency. In this regard, iso-octane is considered as a reference (index 100) in terms of knock resistance against heptane (index 0) [3]. In addition, the oxidation of hydrocarbons forms the basis of most processes for producing polymers (ethylene oxide and propylene oxide, maleic and terephthalic acids, etc.). For instance, iso-octane is the recurring structural subunit of polypropylene and of many polypropionate derived natural products [4–7]. However, the high temperature kinetic mechanism of the oxidation in its propagation and termination phases requires a beforehand initiation phase where a hydrogen is abstracted from the hydrocarbon, before oxidizing its radical form. This

Electronic supplementary material The online version of this article (https://doi.org/10.1007/s00894-019-4105-5) contains supplementary material, which is available to authorized users.

✉ Aziz Aboulmouhajir
aboulmouhajir@gmail.com

[1] Team of Molecular Modelling and Spectroscopy, Faculty of Sciences, University of Chouaib Doukkali, El Jadida, Morocco

[2] Structural Chemistry Group, Department of Chemistry, University of Antwerp, Antwerp, Belgium

[3] Organic Synthesis, Extraction and Valorization Laboratory, Team of Extraction, Spectroscopy and Valorization, Sciences Faculty of Ain Chock, University of Hassan II, Casablanca, Morocco

resulted in the idea to study the conformational behavior of the trimethyl-pentanes, and more particularly iso-octane, which has multiple steric environment hydrogens. Through this study, we explored the structural and electronic properties, determined the optimal conformers and the rotational barriers impeding movement between them, and elucidated the impact of the kinetic and interactional components of the molecule on the vibrational spectra (IR/Raman) in liquid phase, using scale factors of local symmetry force constants [8]. The fundamental vibrational modes were performed with their potential energy distributions (PED-s) and attributed to corresponding observed frequencies for the six lowest energy conformers. Nonlinear activity, particularly first hyperpolarizability, the highest occupied molecular orbital (HOMO) and lowest unoccupied molecular orbital (LUMO), molecular electrostatic potential (MEP) [9], natural bond orbital (NBO) analyses [10], and NMR and UV spectra [11, 12] predictions have been also investigated, in order to have not only an insight into electronic properties of this molecule but also to differentiate between its conformers.

The carbon positions for each conformer are well known by evaluating the two central C–C bonds τ_1 = C1–C2–C3–C4 and τ_2 = C2–C3–C4–C5. The torsional angle τ_1 is taken to be positive if, when looking from C2 along the C2–C3 bond, C4 is in the clockwise sense with respect to C1. The initial configuration and backbone torsional angles, as well as the numbering of the carbon atoms, are shown in Fig. 1 [13].

Theoretical characterizations

The set of programs Molpro was used to carry out the ab initio and DFT optimization [14, 15]. Full geometry optimizations were performed using the method of complete relaxation without any symmetry constraint. Standard gradient techniques at Møller–Plesset perturbation method level MP2 and DFT\B3LYP level, which uses the Becke's hybrid exchange functional B3 and the Lee–Yang–Parr nonlocal correlation functional, were calculated using the 6-311++G(d,p) basis set [16–18].

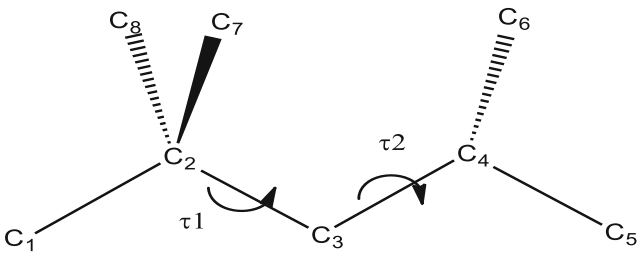

Fig. 1 Backbone torsional angles and the carbon atoms numbering for 2,2,4-trimethylpentane (iso-octane)

Before its relaxed optimization, the total electron energy surface was constructed in steps of 30°, combining the values of τ_1 ranging from 0 to 120° considering the C3v local symmetry of the tert-butyl group and the values of τ_2 ranging from 0 to 360° (Fig. 1). It must be emphasized that the axis of rotation of the tert-butyl group coincides with the central C2C3 bond, while the axis of rotation of the isopropyl group (C2v local symmetry) does not [19]. Only the most stable conformer and the five secondary ones obtained by the optimization calculations are presented in Newman form to give a clear description of the interactions between close groups for each conformer. The transition from one conformer to another needs to overcome the rotational barrier due to the torsion of tert-butyl or isopropyl group, calculated by fixing only the dihedral τ_1 or τ_2 respectively and allowing the variation of all the other parameters. All structures were visualized by employing the Chemcraft 1.8 program [20].

After complete optimization, the vibrational frequencies for these structures were computed from the analytical second derivatives of energy (Hess matrix), at the same levels of methods, with the Gaussian 09 program [21], in order to confirm that they are the true minima on one hand and to carry out their vibrational analysis on the other hand. The unscaled vibrational frequencies are larger than the experimental values because of basis set incompleteness, negligence of electron correlation, and vibrational anharmonicity. Therefore, for reasonable frequency matching, we scaled the ab initio quadratic force constant matrix according to the hessian matrix with the possibility of refinement of the scale factors. Indeed, it is necessary to modulate the quantum force constants by scaling factors C, which are determined from the least-squares adjustment of the calculated frequencies on the experimental ones [22].

$$Fscaled = C^{1/2} F \quad C^{1/2} \tag{1}$$

To help assign vibrational modes, potential energy distributions (PED-s) have been computed using the Gar2ped program [23].

On the basis of the Raman scattering theory, the Raman intensities were also predicted with Gaussian 09, using the following relationship:

$$I_i = \frac{f(\nu_0 - \nu_i)^4 S_i}{\nu_i[1 - \exp(hc\nu_i / k_b T)]} \tag{2}$$

where S_i are the Raman activities, ν_0 is the exciting frequency in cm^{-1}, ν_i is the vibrational wave number of the ith normal mode, h, c, and k_b are the fundamental constants and f is a suitably chosen common normalization factor for all the peak intensities [24, 25].

Natural bonding orbital calculations were performed at B3LYP/6-311++G(d,p) using pop = nbo code as implemented in the Gaussian 09 package. The interactions due to the

overlap between bonding and antibonding orbitals give rise to intramolecular charge transfer (ICT), causing stabilization of the molecule [26]. These interactions are observed as an increase in electron density in antibonding orbital that weakens the respective bond. The delocalization energies associated with the ICT were examined using the Second Order Perturbation Theory analysis of the Fock matrix in the NBO method [27]. For each donor (i) and acceptor (j), the stabilization energy E(2) associated with the delocalization i/j is calculated as:

$$E(2) = \Delta E_{ij} = qi\frac{(F_{ij})^2}{(E_j - E_i)} \tag{3}$$

where q_i is the orbital occupancy, Ei and Ej are the diagonal elements and F(i,j) is the off-diagonal NBO Fock matrix element [28].

The calculations of polarizability α and first-order hyperpolarizibility β were performed on the optimized geometry to understand the nonlinear optical (NLO) behavior of iso-octane conformers [29]. Their electronic energy sensitivity to an external electric field Fi is expressed as follows:

$$E = E^{\circ} - \mu_i F_i - \frac{1}{2}\alpha_{ij}F_iF_j - \frac{1}{6}\beta_{ijk}F_iF_jF_k \tag{4}$$

where E^o is the electronic energy of the unperturbed molecule, Fi is the external field at the origin, μ_i, α_{ij}, and β_{ijk} are the components of dipole moment, polarizability, and first-order hyperpolarizability, respectively. The total static dipole moment μ, the mean polarizability α_0, the anisotropy of the polarizability Δα, and the mean first-order hyperpolarizability β_0, using the x, y, and z components are defined as [30–32]:

$$\mu = \left(\mu_x^2 + \mu_y^2 + \mu_z^2\right)^{1/2} \tag{5}$$

$$\alpha_0 = (\alpha_{xx} + \alpha_{yy} + \alpha_{zz})/3 \tag{6}$$

$$\Delta\alpha = 2^{-1/2}\left[\begin{array}{l}(\alpha_{xx} - \alpha_{yy})^2 + (\alpha_{yy} - \alpha_{zz})^2 + \\ (\alpha_{zz} - \alpha_{xx})^2 + 6\alpha_{Xy}^2 + 6\alpha_{XZ}^2 + 6\alpha_{yZ}^2\end{array}\right]^{1/2} \tag{7}$$

$$\beta_o = \left[\begin{array}{l}(\beta_{xxx} + \beta_{xyy} + \beta_{xzz})^2 + \\ (\beta_{yyy} + \beta_{yzz} + \beta_{yxx})^2 + \\ (\beta_{zzz} + \beta_{zxx} + \beta_{zyy})^2\end{array}\right]^{1/2} \tag{8}$$

Besides this work, we predicted ^{13}C and ^{1}H NMR chemical shifts. It is well known that the inductive attractor effect (-I), attracting and distancing electrons from their nucleus, decreases electron density and electronic diamagnetism near the nucleus. To this diamagnetism, a screen constant σ_i is associated. It reflects the degree of shielding of the nucleus with regard to its environment, thus giving rise to a peak of resonance, in accordance with NMR fundamental formula.

$$\nu_i = \gamma B_0(1 - \sigma_i) \tag{9}$$

where γ is the gyromagnetic ratio and B_0 is the magnetic field intensity, and the chemical shift, which is the resonant frequency of a nucleus relative to the tetramethylsilane (TMS) standard in a magnetic field, is given by:

$$\delta = \sigma_{ref} - \sigma_{i.} \tag{10}$$

Therefore, the lower the screen constant (deshielding effect), the larger the chemical shift δ and the lower the field of NMR signal.

It should also be noted that, in addition to the negative sensitivity of the nucleus chemical shift to its surrounding electron density and thus to the electronegativity of the neighboring atoms, it is favorably sensitive to magnetic anisotropy resulting from the electronic current associated with the delocalization of electrons.

For iso-octane, we calculated the chemical shift of both ^{13}C and ^{1}H for the six A–F conformers, in order to differentiate them, once more, and to verify the compatibility of their values to the experiment. The structure of the six conformers was optimized at the B3LYP/6-311+G(d,p) level. Then, the gauge-including/invariant atomic orbital (GIAO) [33] ^{1}H and ^{13}C chemical shift calculations are performed by the same basis set in $CDCl_3$ solution by IEFPCM model [34].

On the other hand, because DFT and time dependent DFT (TD-DFT) can offer a highly acceptable prediction of the electronic and optical properties, the excitation energies of the title molecule were also performed at TD-B3LYP/6-311++G(d,p), in the gas phase and in DMSO solvent, to reproduce the UV spectrum [35, 36].

Results and discussion

Geometry optimization and conformational stability

Taking into account the symmetry of the tert-butyl group and the coincidence of its local symmetry axis with the rotational bond C2C3 contrary to the isopropyl group, the exploration of the iso-octane conformational space generated 48 conformations combining τ_1 and τ_2 values as presented in Fig. 2.

Ab initio MP2/6-311++G(d,p) and B3LYP/6-311++G(d,p) levels provide two nearly equivalent minima A and B in terms of interactions, two first secondary conformers C and D in a range of 0.6 kcal mol^{-1}, and two nearly equivalent high secondary conformers in a range of 3.6 kcal mol^{-1}, the conformers C and D are equivalent by effect of symmetry with respect to the trans main chain, whereas A and B or E and F are equivalent in terms of interactions between atoms only. In

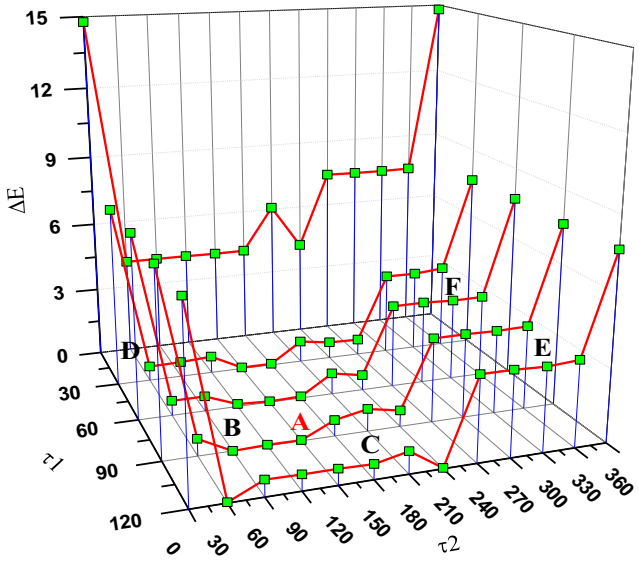

Fig. 2 Distribution of the 2,2,4-trimethylpentane conformers with respect to their initial torsion angles τ1 and τ2 by B3LYP/6-311++G(d,p) method

addition to torsional angles differences between conformers, the conformational variability also concerns the CCC angles. It reaches a maximum value (6°) for the central angle C2C3C4 for both methods.

By comparing B3LYP/6-311++G(d,p) and MP2/6-311++G(d,p), it is noteworthy that the former is slightly more stabilizing as the energy is decreased about 655 kcal mol^{-1}, while the latter renders values of C2C3, C3C4 bond lengths and C2C3C4 angle, for the six conformers A–F, shorter by about 0.01 Å and 1° than the B3LYP ones, while almost all the other bond lengths and angles remain unchanged for the two methods. Regarding the dihedral angles, we noticed that the variation between angles does not exceed 4° from one method to another, especially for C and D conformers (Table 1, Fig. 3). Additionally, the computed bond lengths and bond angles of the titled compound were compared with their experimental data [37]. The MP2/6-311++G(d,p) values obtained for the angle α (C1–C2–C3) and distance r (C1–C2) are closer to the experiment compared to the B3LYP/6-311++G(d,p) values (Table 1).

In the light of the optimization results, the syn-pentane interaction, which appears between every fifth carbon atom, is considered the major factor influencing the stability of conformers. This explains the weakness of strain caused by tert-butyl/isopropyl interaction in A and B conformers compared to the secondary ones (Fig. 3).

Isopropyl barriers to internal rotation

The rotational barriers between the most stable conformers A and B or between secondary conformers C and E or D and F and their correspondent inversion barriers were evaluated at both MP2 and B3LYP using 6-311++G(d,p) basis set. All these transitions A ($\tau_1 = 55$, $\tau_2 = 140$) → B ($\tau_1 = 66$, $\tau_2 = 96$), C ($\tau_1 = 42$, $\tau_2 = 63$) → E ($\tau_1 = 74$, $\tau_2 = -54$), and D ($\tau_1 = 78$, $\tau_2 = 170$) → F ($\tau_1 = 48$, $\tau_2 = -76$) have the particularity of being one-dimensional rotation around C3C4 bond, knowing that the torsion angle τ_2 was kept at constant value, in 5° intervals, while all the other angles and bond lengths were optimized. Moreover, with τ_1 near 60, the evolution of the rotational transition throughout the total interval of τ_2 [−180, 170] enabled us to identify the equivalence between C → E and D → F rotational transitions, due to a Cs symmetry of the molecule for $\tau_2 = 120$.

According to the results collected in Table 2 and presented in Figs. 4 and 5, the MP2/6-311++G(d,p) or B3LYP /6-311++G(d,p) rotational barrier of A → B transition and its inversion barrier are very weak compared to their corresponding C → E or D → F transitions. By comparing the two methods, MP2/6-311++G(d,p) C → E or D → F rotational barriers and their corresponding inversion barriers were found to be larger by about 1 kcal mol^{-1} than B3LYP/6-311++G(d,p) values. Obviously, the values of C → E or D → F rotational barriers and their inversion barriers are high because they have to overcome the strong interaction of the tert-butyl and isopropyl groups.

Considering the absence of experimental rotational barriers for iso-octane and the abundance of experimental data for iso-butane (methylpropane), we assessed the consistency of the methods MP2/6-311++G(d,p) and B3LYP/6-311++G(d,p) by evaluating the internal rotation barrier of methyl with respect to the only existing stable conformation of iso-butane (Fig. 1S in Supplementary information). We thus found that the 3.56 kcal mol^{-1} value of the MP2/6-311++G(d,p) rotation barrier is closer to the experiment than 3.24 kcal mol^{-1}, calculated by B3LYP/6-311++G(d,p), since its evaluation from microwave spectra [38] and from two thermodynamic results [39] gives respectively 3.90, 3.62, and 3.87 kcal mol^{-1}. However, apart from the calculation of the rotation barrier, which is part of the kinetic study, the B3LYP/6-311++G(d,p) is more stabilizing in terms of energy and thus thermodynamically and spectroscopically. This is why the DFT prediction of electronic and spectroscopic properties was chosen.

HOMO–LUMO and molecular electrostatic potential (MEP) analyses

The energy gap between HOMO and LUMO orbitals is directly related to chemical softness and the chemical reactivity of a molecule in the frontier molecular orbitals (FMOs) theory [40]. The huge gap explains the high stability and low reactivity, as is the case, for instance, with the saturated hydrocarbons and their oxidation processes.

Table 1 Computed geometrical parameters of the six lowest energy conformers of 2,2,4-trimethylpentane (r is bond length in Angstroms, α and δ are valence and dihedral angles in degrees, Exp: from ref. [37])

Parameters	MP2/6-311++G(d,p)						B3LYP/6-311++G(d,p)						Exp
	A	B	C	D	E	F	A	B	C	D	E	F	
E (kcal mol^{-1})	−197508,6	−197508,6	−197508	−197508	−197505,1	−197505,1	−198163,6	−198163,6	−198163	−198163	−198160	−198160	
ΔE	0	0,001	0,56	0,56	3,49	3,49	0	0,001	0,60	0,60	3,58	3,58	
δ(C1-C2–C3–C4)	56,40	66,14	45,58	77,92	74,11	49,85	55,60	66,93	42,05	81,52	76,24	47,90	
δ(C2–C3–C4–C5)	140,38	96,33	66,99	169,64	−54,46	−75,98	139,00	98,44	62,73	174,80	−52,59	−76,68	
δ(C2–C3–C4–C6)	−96,31	−140,36	−169,66	−67,01	75,98	54,47	−98,42	−138,96	−174,80	−62,74	76,67	52,58	
δ(C4–C3–C2–C7)	−66,15	−56,40	44,10	−44,10	−48,50	48,50	−66,94	−55,60	40,60	−40,60	−46,60	46,60	
δ(C4–C3–C2–C8)	55,89	−55,90	−77,93	−45,59	−49,86	−74,10	54,94	−54,95	−81,52	−42,04	−47,91	−76,25	
α(C1–C2–C3)	108,1	110,1	111,1	112,2	112,2	113,2	107,8	110,3	111,3	112,4	112	113,2	109,5
α(C2–C3–C4)	116,9	116,9	120,1	120,1	123,2	123,2	118,3	118,3	121,1	121,1	124,1	124,1	
α(C3–C4–C5)	110,6	111,7	114,4	108,6	115,2	114,3	110,8	112,3	114,9	108,9	115,7	114,3	
α(C3–C4–C6)	111,7	110,6	108,6	114,4	114,1	115,2	112,3	110,8	108,9	114,9	114,3	115,7	
α(C1–C2–C7)	108,6	108,6	108,7	107,5	107,5	108,2	108,6	108,6	108,6	107,6	107,6	108,2	
α(C1–C2–C8)	108,8	109,5	110,1	110,1	109,3	109,3	108,7	109,3	109,7	109,7	109,2	109,2	
α(C5–C4–C6)	109,8	109,8	109,4	109,4	110,5	110,5	109,9	109,9	109,6	109,6	110,7	110,7	
α(C7–C2–C3)	110,1	108,2	107,2	107,2	106,4	106,4	110,3	107,8	107,2	107,2	106,5	106,5	
α(C8–C2–C3)	111,7	111,7	112,2	111,1	113,2	112,5	112,1	112,1	112,4	111,3	113,2	112,4	
α(C7–C2–C8)	109,5	108,8	107,5	108,7	108,2	107,5	109,3	108,7	107,6	108,6	106,5	107,6	
r(C1–C2)	1,534	1,534	1,532	1,535	1,536	1,533	1,542	1,541	1,542	1,542	1,543	1,542	1,537
r(C2–C3)	1,542	1,542	1,546	1,546	1,548	1,548	1,554	1,554	1,557	1,557	1,559	1,559	
r(C3–C4)	1,544	1,544	1,537	1,537	1,545	1,545	1,551	1,551	1,546	1,546	1,554	1,554	
r(C4–C5)	1,532	1,532	1,531	1,533	1,531	1,534	1,537	1,537	1,536	1,539	1,536	1,539	
r(C4–C6)	1,532	1,532	1,533	1,531	1,534	1,531	1,537	1,537	1,539	1,536	1,539	1,536	
r(C2–C7)	1,534	1,534	1,536	1,536	1,537	1,537	1,541	1,542	1,544	1,544	1,545	1,545	
r(C2–C8)	1,532	1,532	1,535	1,532	1,533	1,536	1,541	1,541	1,542	1,542	1,543	1,543	

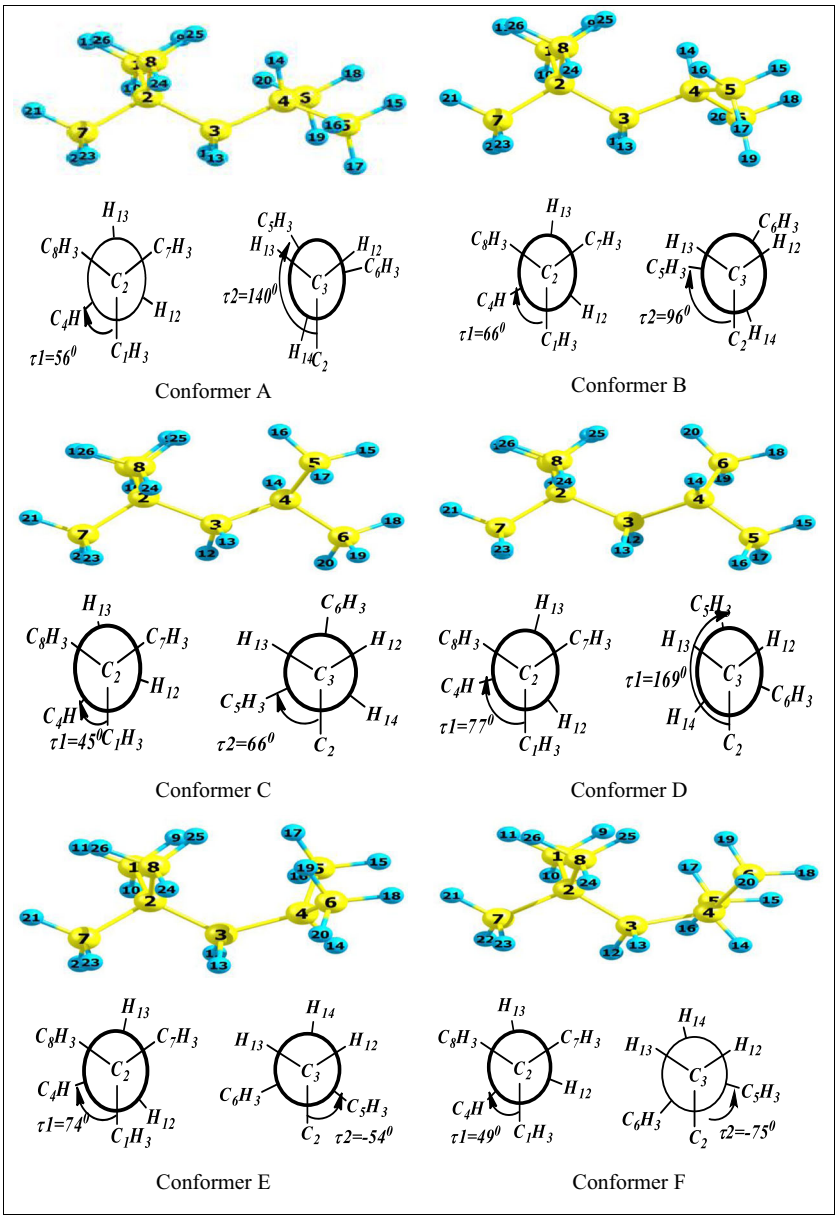

Fig. 3 Newman projections of the six lowest energy conformers of 2,2,4-trimethylpentane

The values of HOMO, LUMO, energy gap, and softness for the six conformers are collected in Table 3. The pictorial diagram of HOMO and LUMO energy levels is presented in Fig. 6. The energy gap between MOs is 7.90 ev in A and B conformers, 7.85 ev in C and D conformers, and 7.65 ev in E and F conformers, suggesting that the molecule is slightly soft in the latter form. This is confirmed by their larger electronic distribution in LUMO orbitals compared to the other conformers.

Knowing that the red color shows the lowest MEP value (negative) and the blue color the highest one (positive), while the yellow color indicates intermediary potential [41], we noticed that the electrostatic molecular potential also presented in Fig. 6 is almost identical for all conformers, as the yellow color concerns all the skeleton carbon atoms and blue color concerns all hydrogen atoms.

Table 2 Values (kcal mol^{-1}) of possible rotational barriers to torsional angle τ2 = C2C3C4C5 and their correspondent inversion (in parentheses) for 2,2,4-trimethylpentane

	A → B	C → E	D → F
B3LYP/6-311++G(d, p)	0.2 (0.18)	6.57 (3.74)	6.6 (3.77)
MP2/6-311++G(d, p)	0.2 (0.17)	7.86 (4.76)	7.61 (4.6)

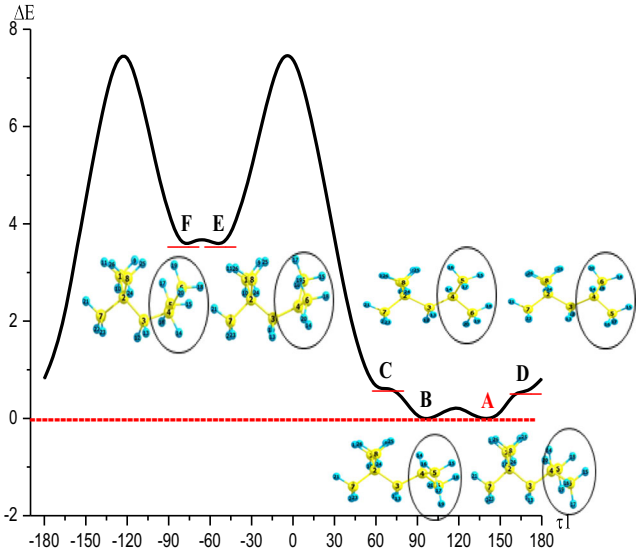

Fig. 4 Evolution of B3LYP/6-311++G(d,p) rotational barrier to torsional angle τ2 = C2C3C4C5 for 2,2,4-trimethylpentane

Natural bond orbital analysis

The E(2) stabilization energy indicates the direct relationship between the intensity of ICT and the interaction between bonding and antibonding orbitals. The calculated values of E(2) presented in Table S1 (Supplementary information) have several particularities:

- All electronic transfers took place between σ type molecular orbitals.
- The E(2) high values reflecting high ICT between bonding orbital σ_{ab} and antibonding orbital σ^*_{cd} concern the ab and cd bonds in trans position.
- The larger values of E(2) concern the σ_{CH}–σ^*_{CC} interactions, especially for σ(C3–H12)–σ*(C2–C8) (B and E conformers) and σ(C3–H13)–σ*(C1–C2) (A and F conformers) as they exceed 4 kcal mol^{-1}.
- σ(C3–H12)–σ*(C4–C6) and σ(C3–H13)–σ*(C4–C5) lead large values of E(2) both for E and for F conformers as C4–C6 and C4–C5 are in trans position vis-a-vis of C3–H12 and C3–H13, respectively.
- The interactions σ_{CH}–σ^*_{CH} and σ_{CC}–σ^*_{CH} are intense but less intense than the σ_{CH}–σ^*_{CC} interactions and are localized in the interval of 2 to 4.5 kcal mol^{-1}.

Considering the branching of the iso-octane, we were particularly interested in the intramolecular interaction of carbon skeleton σ_{CC}–σ^*_{CC} with the aim of differentiating between conformers. We noticed the interaction of σ_{C2C7} of the tert-butyl group with σ^*_{C3C4} for all six conformers A–F had values within the interval of 2.5 to 3 kcal mol^{-1}. It is the same for the interaction of σ_{C4C5} of the isopropyl group with σ^*_{C2C3} having the values 1.42 and 2.76 kcal mol^{-1} for the conformers A and D, respectively, and σ_{C4C6}–σ^*_{C2C3} interaction having the values 1.50 and 2.76 kcal mol^{-1} for B and C conformers, respectively. It is worth noting that the reverse interaction between the bonding and antibonding orbitals is correspondingly diminished.

From E(2) values analysis, it could be concluded that the conformational flexibility affects intramolecular charge transfers of natural bond orbitals.

First-order hyperpolarizability and nonlinear optics analysis

As presented in Table 4, the highest value of dipole moment is observed for A and B conformers, this value is equal to 0.58 Debye. The values of static polarizability or the mean polarizability α_0 are very close for the six conformers A–F, while the total polarizability or the anisotropy of the polarizability $\Delta\alpha$ is relatively lower for the two most stable conformers A–B compared to the secondary ones. The magnitude that is more sensitive to conformers is the first-order hyperpolarizability (β_0). Indeed, the B3LYP/6-311++G(d,p) first-order hyperpolarizability values are, respectively, 466.452 10^{-33} esu and 476.250 10^{-33} esu for A and B conformers, 601.951 10^{-33} esu and 603.320 10^{-33} esu for C and D conformers, and 789.880 10^{-33} esu and 793.270 10^{-33} esu for E and F conformers. β_0 of A and B conformers is greater than that of urea, taken as a reference [27, 42, 43] of about 27%, while β_0 of the secondary conformers C–F is almost two times larger than that of urea leading to moderate nonlinear optics activity of the title molecule.

Carbon ^{13}C and proton ^{1}H NMR spectra prediction

The theoretical relative ^{13}C and ^{1}H-NMR chemical shift values are reported in ppm as shown in Tables 5 and 6 for all the conformers and illustrated for the most stable conformer A (Fig. 7). They were also correlated with natural NPA charges and compared with the experimental data where the skeleton carbons are overlapping with chemical shift values from 25 to 55 ppm and hydrogens from 0.89 to 1.65 ppm [44, 45].

We first observed the high value exceeding 50 ppm of the central carbon C3, the point of connection between the tert-butyl and isopropyl groups. In the same direction, with a value of about 40 ppm, δ_{C2} of central tertiary butyl carbon exceeds those of the connected peripheral carbons (C1, C7, and C8), and with a value ranging from 30 to 35 ppm, δ_{C4} of central isopropyl carbon exceeds those of the connected peripheral

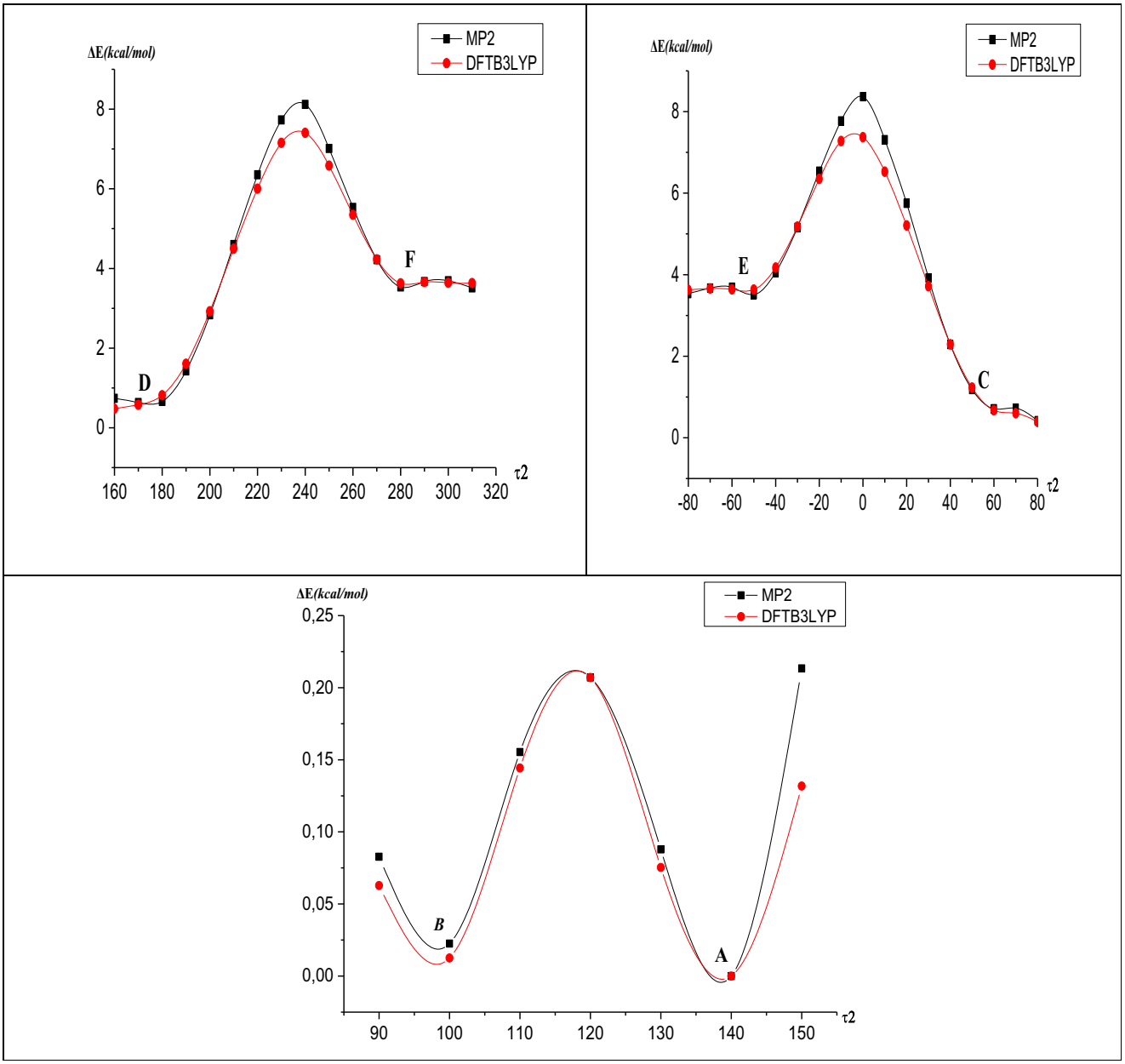

Fig. 5 B3LYP/6-311G++(d,p) and MP2/6-311G++(d,p) rotational barriers to torsional angle τ2 = C2C3C4C5 for 2,2,4-trimethylpentane

Table 3 The HOMO–LUMO energy gap and softness for the six lowest energy conformers of 2,2,4-trimethylpentane

Conformers	HOMO	LUMO	ΔE	S
A	−82.029	−0.3000	79.032	0.2531
B	−82.031	−0.3000	79.032	0.2531
C	−81.672	−0.3137	78.535	0.2547
D	−81.672	−0.3137	78.535	0.2547
E	−79.898	−0.3391	76.507	0.2614
F	−79.898	−0.3391	76.507	0.2614

carbons (C5 and C6). These results show clearly that the electronic depletion concerns the central skeletal carbons. Indeed, the natural NPA atomic charge of skeletal carbons varies from −0.1 to −0.4, whereas it is of the order of −0.6 for all peripheral carbons (Tables 5 and 6). We also noted the slightly elevated value of δ_{C7} compared to the other peripheral carbons due to its coplanarity with the C2, C3, and C4 carbons, giving its electrons more mobility. On the other hand, the highest ^{1}H-NMR chemical shift (varying from 1.5 to 1.9 ppm going from A to F) was found for H14, which is bound

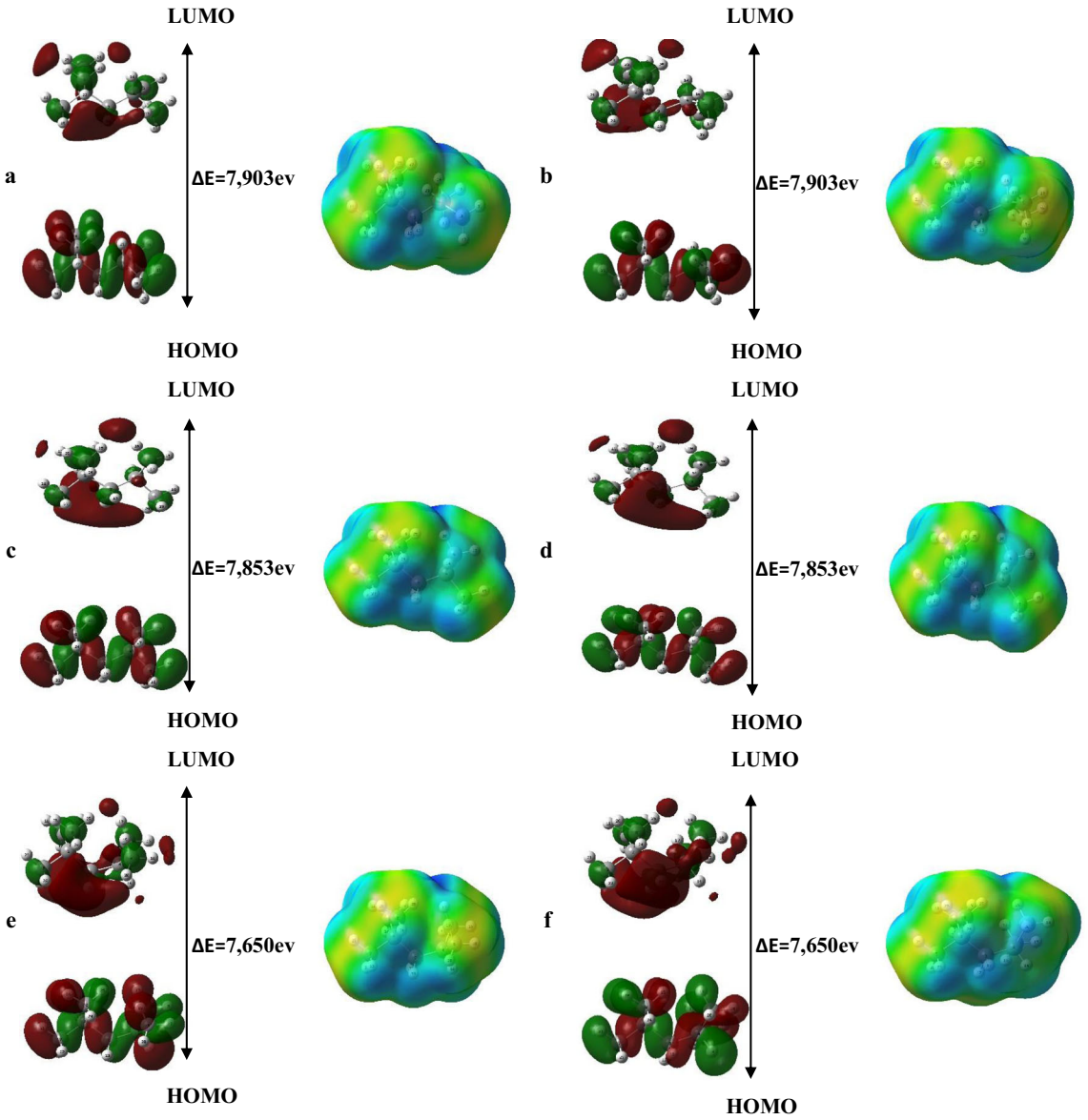

Fig. 6 Pictorial separation of electronic energy levels with frontier MOs and molecular electrostatic potential plots of 2,2,4-trimethylpentane conformers

Table 4 The electric dipole moment μ, static polarizability α_0, anisotropy of the polarizability $\Delta\alpha$, and first-order hyperpolarizability of 2,2,4-trimethylpentane by the B3LYP/6-311++G(d,p) method

Conformers	μ	α_0 esu(10^{-24})	$\Delta\alpha$ esu(10^{-24})	β_0 esu(10^{-33})
A	0.0584	14.780	2.385	466.452
B	0.0582	14.783	2.394	476.250
C	0.2028	14.795	2.183	601.951
D	0.2018	14.792	1.984	603.320
E	0.1236	14.688	0.969	789.880
F	0.1261	14.690	1.251	793.270

(μ: debye; α: 1 au = 0.1482×10^{-24} esu; β: 1 a u. = 8.6393×10^{-33} esu)

to the isopropyl C4 carbon, is correlated with the lowest natural charge (0.184) that is less than the other charges by about 0.014.

Knowing that the different conformers are differentiated by the configuration of the isopropyl group, we noted that the chemical shifts δ_{C5} and δ_{C6} are of the order of 26 ppm for the conformers A and B while they exchange their values from C (δ_{C5} = 22 and δ_{C6} = 26 ppm) to D and from E (δ_{C5} = 22 and δ_{C6} = 24 ppm) to F, with a higher chemical shift affecting the carbon that is closer to the plane C7C2C3C4. In addition, the H14 of the isopropyl group is also a source of differentiation, since the value of its chemical shift is respectively of the order of 1.5, 1.7, and 1.9 ppm for (A, B), (C, D), and (E, F).

Table 5 The experimental and calculated ^{13}C-NMR isotropic chemical shifts and natural population analysis charge of all conformers A–F

	A		B		C		D		E		F		Expt
	NPA	δ	NPA	δ	NPA	δ	NPA	δ	NPA	δ	NPA	δ	δ
C1	−0.566	30.7	−0.571	27.33	−0.574	26.11	−0.568	29.62	−0.570	30.63	−0.572	28.69	30.16
C2	−0.087	36.75	−0.088	36.66	−0.092	36.34	−0.092	36.35	−0.093	38.71	−0.093	38.71	31.1
C3	−0.370	53.1	−0.370	54.41	−0.369	54.89	−0.369	54.9	−0.367	52.22	−0.367	52.22	53.28
C4	−0.237	29.22	−0.237	28.9	−0.229	30.85	−0.229	30.85	−0.222	35.4	−0.223	35.4	24.73
C5	−0.563	26.32	−0.566	24.89	−0.570	22.55	−0.564	26.51	−0.572	21.81	−0.569	24.17	25.51
C6	−0.566	25.55	−0.563	26.14	−0.564	26.5	−0.570	22.56	−0.569	24.17	−0.572	21.81	25.51
C7	−0.571	32.27	−0.566	33.46	−0.565	35.29	−0.565	35.29	−0.565	36.2	−0.565	36.19	30.16
C8	−0.574	26.19	−0.573	27.23	−0.568	29.61	−0.574	26.11	−0.572	28.69	−0.570	30.63	30.16

Moreover, the experimental values of δ_{C5}, δ_{C6}, and δ_{H14} are more compatible with the conformers A and B than the C, D, E, and F conformers, whereas the calculation of the correlation between observed and theoretical chemical shifts, particularly in ^{13}C-NMR (Fig. 8, Table 7), rejected categorically the conformers E and F as stable conformers. Indeed, they are not only of lower stability but also require a relatively high barrier of rotation.

Electronic UV spectra

Time-dependent density functional theory (TD-DFT) is calculated on the optimized geometries by using the same basis sets and hybrid functional, in order to extract the ground to excited state transitions, the excitation energies, and oscillator strengths, with respect of the Franck–Condon principle [46].

Table 6 The experimental and calculated ^{1}H-NMR isotropic chemical shifts and natural population analysis charge of all conformers A–F

	A		B		C		D		E		F		Expt
	NPA	δ	NPA	δ	NPA	δ	NPA	δ	NPA	δ	NPA	δ	δ
H9	0.198	1.158	0.197	1.22	0.199	1.057	0.198	1.38	0.201	1.394	0.197	1.146	0.891
H10	0.198	0.698	0.198	0.602	0.199	0.729	0.198	0.746	0.197	0.787	0.200	0.923	0.891
H11	0.198	0.705	0.199	0.693	0.200	0.795	0.197	0.737	0.197	0.762	0.198	0.797	0.891
H12	0.195	0.94	0.196	1.048	0.196	1.272	0.192	0.918	0.196	1.488	0.195	1.378	1.122
H13	0.196	1.06	0.195	1.029	0.193	0.917	0.196	1.273	0.196	1.378	0.196	1.488	1.122
H14	0.184	1.515	0.184	1.548	0.185	1.707	0.185	1.708	0.182	1.917	0.182	1.918	1.659
H15	0.197	0.878	0.196	0.877	0.198	0.859	0.198	0.938	0.199	0.999	0.197	0.965	0.907
H16	0.197	0.918	0.200	1.194	0.195	1.379	0.197	0.86	0.199	1.135	0.196	1.011	0.907
H17	0.192	0.778	0.192	0.53	0.194	0.505	0.192	0.732	0.190	0.993	0.194	1.218	0.907
H18	0.196	0.895	0.197	0.874	0.198	0.938	0.198	0.859	0.197	0.965	0.199	0.999	0.907
H19	0.192	0.538	0.193	0.748	0.192	0.732	0.194	0.506	0.194	1.218	0.190	0.993	0.907
H20	0.199	1.335	0.197	0.915	0.197	0.86	0.195	1.379	0.196	1.011	0.199	1.135	0.907
H21	0.199	0.867	0.198	0.853	0.198	0.754	0.198	0.755	0.198	0.658	0.198	0.658	0.891
H22	0.198	0.775	0.198	0.814	0.197	0.746	0.199	0.94	0.198	0.9	0.197	0.816	0.891
H23	0.197	0.825	0.198	0.817	0.199	0.94	0.197	0.746	0.197	0.816	0.198	0.9	0.891
H24	0.199	0.601	0.198	0.735	0.198	0.745	0.199	0.73	0.200	0.923	0.197	0.787	0.891
H25	0.199	1214	0.199	1.027	0.198	1.379	0.198	1.057	0.197	1.146	0.201	1.395	0.891
H26	0.200	0.656	0.199	0.731	0.197	0.736	0.200	0.796	0.198	0.797	0.197	0.762	0.891

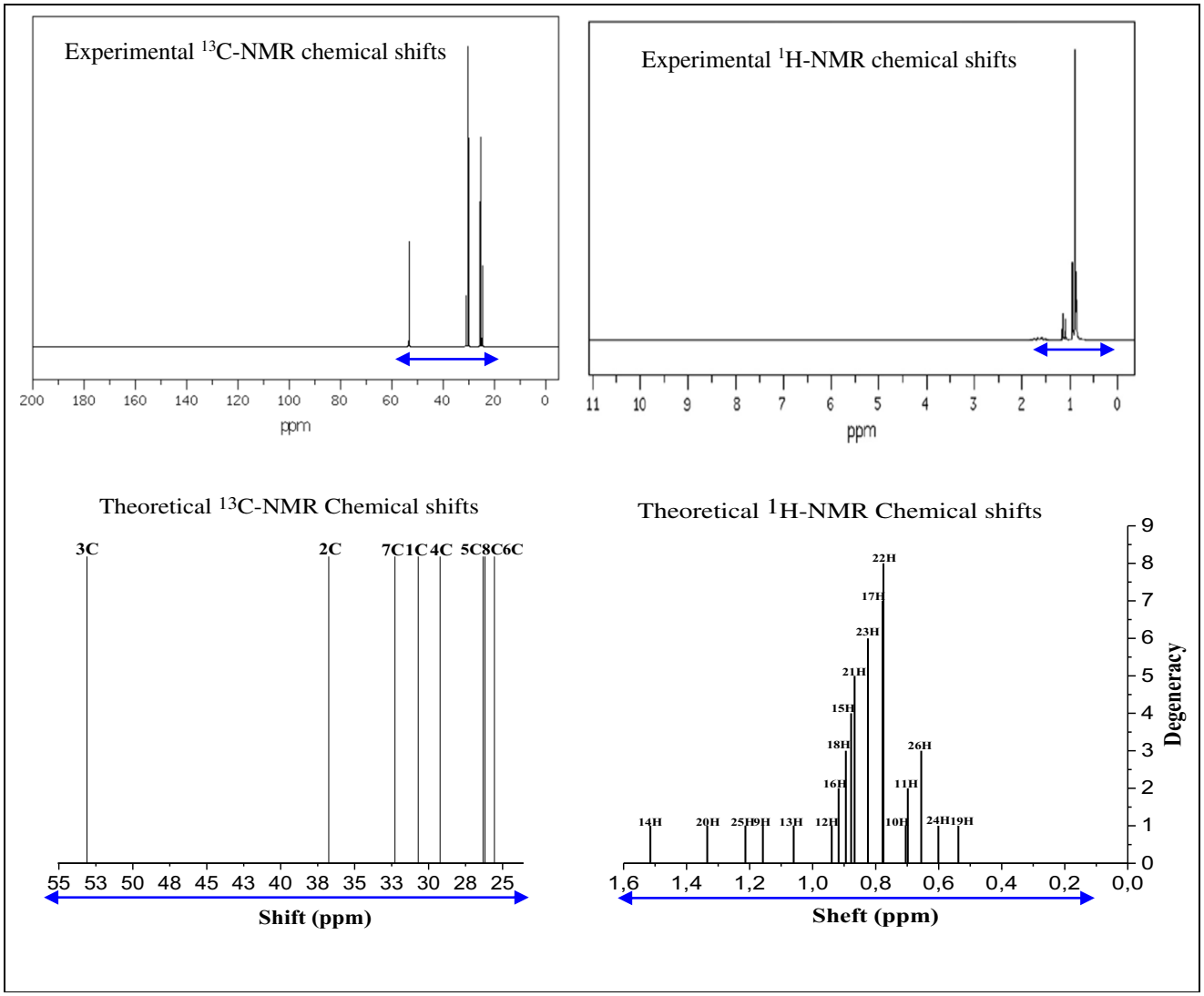

Fig. 7 The experimental and calculated ^{13}C and ^{1}H-NMR chemical shifts (ppm) of the most stable conformer A

The TD-DFT electronic transitions of iso-octane was calculated without experimental results. Indeed, the saturated form of this molecule gives it a high HOMO–LUMO energy gap (almost 8 ev), making it more stable and the σ–σ* electronic transition more difficult (shorter wavelength of absorption maxima).

The excitation wavelengths (λ), energies (E), oscillator strengths (f), and the assignment of electronic excitation of each isolated iso-octane conformer (A–F) and in solvent DMSO are presented in Table 8, while the theoretical electronic spectrum is shown in Fig. 9.

The results of conformers A and B disclose three relatively intense electronic transition peaks at 163, 167, and 171 nm, with the respective values of the oscillator strength 0.081, 0.044, and 0.062 assigned respectively to HOMO-2 -> LUMO, HOMO-1 -> LUMO and HOMO -> LUMO excitation, as main contributions. The conformers C and D exhibit the same main contributions with a slight shift not exceeding the unit for (λ) and 0.2 for (f), compared to A and B conformers. However, the transition HOMO-1 -> LUMO has been submitted to a (λ) shift of 2 nm, from C or D to E or F, while specifically for these latters the transition HOMO -> LUMO+1 appears (contribution of about 70%) at 165 nm with (f) about 0.05 au.

On the other hand, the use of DMSO solvent has a noticeable effect on (f) which increases by about 20 to 25% for all the conformers in addition to the reappearance of the HOMO -> LUMO excitation at 177 nm even with weak strength of about 0.02, and the disappearance of HOMO-2 —> LUMO transition, for E and F conformers.

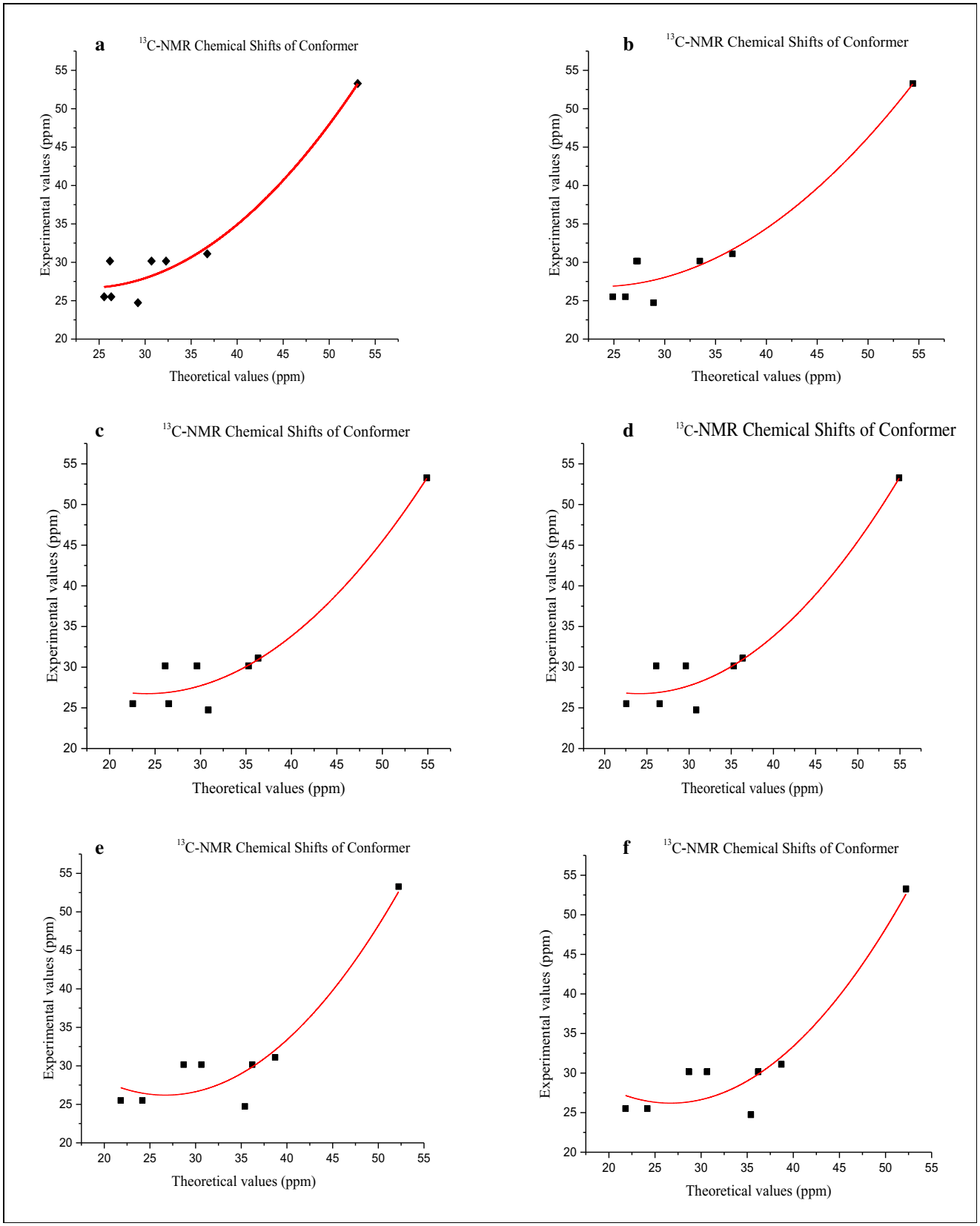

Fig. 8 The observed and calculated ^{13}C-NMR chemical shifts correlation of all A–F conformers

Table 7 The adjusted R-squared between observed and calculated ^{13}C-NMR chemical shifts for all A–F conformers

Conformers	A	B	C	D	E	F
Adjusted. R-squared	0.93265	0.92862	0.92503	0.92507	0.87987	0.87986

Temperature sensitivity and scaled vibrational assignment of conformers

As it is commonly accepted that the conformational behavior of Raman and IR spectra is very sensitive to temperature, mainly at low frequencies, we recorded, in our earlier work [47], the Raman spectrum of iso-octane in liquid phase below 600 cm^{-1} in the temperature range from 293 to 183 K. As is shown in Fig. 10, if we exclude the refinement of bands caused by cooling of the sample, we did not notice any exchange between bands in terms of intensity, thereby removing any possibility of conformational change. It should be noted that the infrared spectrum between 200 and 600 cm^{-1} does not show any bands that are inactive in the Raman spectrum. For this reason, temperature sensitivity of the infrared region was not considered.

The absence of temperature-sensitive bands in the spectra of this isomer can be related to the fact that the vibrational frequencies of the two most stable conformers A and B are not sufficiently shifted from the secondary ones. To confirm this, the scaled vibrational normal modes calculations were made leading us to the harmonic frequencies of vibrations adjusted to the observable frequencies as well as the distribution of the potential energy for each calculated normal mode. To highlight the local symmetry of the carbon skeleton, we considered the symmetry coordinates based on the C_3v local symmetry of the tert-butyl group (DS TS DD SD DR CCC), while the C_2v symmetry of the isopropyle group is ignored because the rotation axis does not coincide with the CC rotation. All used symmetry coordinates are derived from internal coordinates and detailed in Table S2 (Supplementary information).

Table 8 Calculated absorption wavelength (λ) (nm), excitation energies E (ev), and oscillator strengths (au) of six conformers using the B3LYP/311++G(d,p) level

Confs	Gas			Main contribution	DMSO			Main contribution
	λ (nm)	E (ev)	f (a,u)		λ (nm)	E (ev)	f (au)	
A	170.77	7.26	0.062	HOMO ---> LUMO (70%)	170.7	7.263	0.079	HOMO ---> LUMO (70%)
	167.11	7.419	0.044	HOMO-1 ---> LUMO (69%)	167.15	7.417	0.06	HOMO-1 ---> LUMO (69%)
	162.84	7.614	0.081	HOMO-2 ---> LUMO (70%)	162.97	7.608	0.109	HOMO-2 ---> LUMO (70%)
B	170.76	7.261	0.062	HOMO ---> LUMO (70%)	170.69	7.264	0.079	HOMO ---> LUMO (70%)
	167.11	7.419	0.044	HOMO-1 ---> LUMO (70%)	167.16	7.417	0.06	HOMO-1 ---> LUMO (70%)
	162.85	7.614	0.081	HOMO-2 ---> LUMO (70%)	162.97	7.608	0.109	HOMO-2 ---> LUMO (69%)
C	172.09	7.205	0.053	HOMO ---> LUMO (70%)	171.91	7.212	0.069	HOMO ---> LUMO (70%)
	166.64	7.44	0.060	HOMO-1 ---> LUMO (70%)	166.62	7.441	0.08	HOMO-1 ---> LUMO (70%)
	163.37	7.589	0.061	HOMO-2 ---> LUMO (69%)	163.44	7.586	0.082	HOMO-2 ---> LUMO (69%)
D	172.09	7.205	0.053	HOMO ---> LUMO (70%)	171.91	7.212	0.069	HOMO ---> LUMO (70%)
	166.64	7.44	0.06	HOMO-1 ---> LUMO (70%)	166.62	7.441	0.08	HOMO-1 ---> LUMO (70%)
	163.36	7.589	0.061	HOMO-2 ---> LUMO (69%)	163.44	7.586	0.082	HOMO-2 ---> LUMO (69%)
E	168.17	7.373	0.062	HOMO-1 ---> LUMO (70%)	177.39	6.99	0.019	HOMO ---> LUMO (70%)
	165.07	7.511	0.051	HOMO ---> LUMO+1 (69%)	168.19	7.372	0.082	HOMO-1 ---> LUMO (70%)
	163.95	7.562	0.084	HOMO-2 ---> LUMO (70%)	165.44	7.494	0.064	HOMO ---> LUMO+1 (68%)
F	168.17	7.373	0.062	HOMO-1 ---> LUMO (69%)	177.38	6.99	0.019	HOMO ---> LUMO (70%)
	165.07	7.511	0.051	HOMO ---> LUMO+1 (68%)	168.19	7.372	0.082	HOMO-1 ---> LUMO (70%)
	163.95	7.562	0.084	HOMO-2 ---> LUMO (70%)	165.43	7.495	0.064	HOMO ---> LUMO+1 (68%)

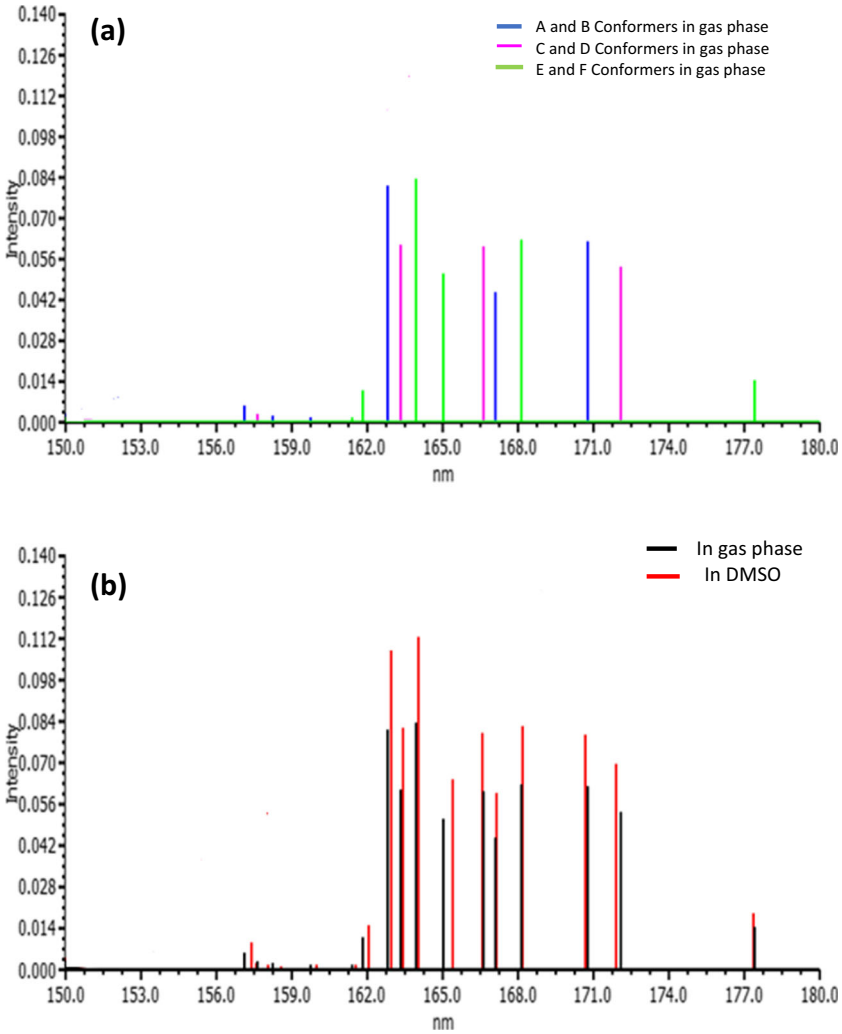

Fig. 9 Theoretical electronic spectrum (oscillator strengths (au) as a function of absorption wavelength (λ) (nm)) in gas phase (**a**) and in DMSO solvent (**b**) for all A–F conformers

The refinement of the ab initio normal modes frequencies has been carried out through the optimization of the scale factors of B3LYP/6-311++G(d,p) force constants for the conformer A (Table 9). For the other less stable conformers, the variation of scale factors compared to A does not exceed 4%. Raman and IR frequencies, in liquid phase, as well as the adjusted calculated frequencies are listed in Table 10. As shown by the temperature sensitivity study of the Raman low frequency region, eliminating any possibility of conformational exchange, all observed frequencies are predicted by scaled normal mode calculation for the most stable conformer A. Thus, only the PED for conformer A is given, all minor contributions (contributions <10%) are eliminated unless they consolidate the preponderant contribution, in this case, even the contributions going down to 5% are considered. On the whole, the computed scaled frequencies are in good agreement with the experimental data leading rms deviation, not exceeding 10 cm^{-1} for all frequencies and 6 cm^{-1} below 1500 cm^{-1}. The comparison between calculated and observed intensities was used, mainly in Raman, to verify the symmetrical character of the calculated mode of vibration. Indeed, the more symmetrical the mode, the higher its Raman intensity.

As the molecule 2,2,4-trimethyl pentane contains five CH3, one CH2, and one CH, its different vibration modes are subdivided into two groups. The first group (18 modes) contains ten degenerates asymmetric stretching CH3ds (in plane and out of plane), five symmetric stretching CH3ts, one asymmetric stretching CH2as, one symmetric stretching CH2ss, and one CH stretching CHs. All these modes are considered pure as long as the complementary contributions are minor and do not exceed 10%. Their respective frequencies are observed and well predicted in the region [2900, 2840] in accordance with the following order: CH3ds > CH2as > CH3ts > CH2ss > CHs, as found in our earlier work and those of Mirkin et al. for some normal and congested alkanes [48]. The second group contains, as pure modes or in combination,

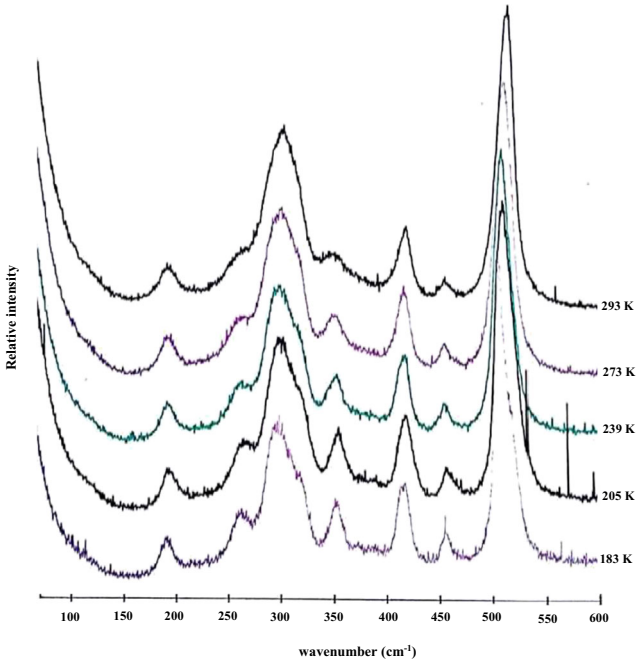

Fig. 10 Observed low frequency Raman spectrum of 2,2,4-trimethylpentane, in liquid phase below room temperature

ten degenerate asymmetric deformations CH3ab (in plane and out of plane), five symmetric deformations CH3sb, five degenerate rocking CH3dr (in plane and out of plane), one CH2sc scissoring, one CH2wa wagging, one CH2tw twisting, one CH2ro rocking, CCH defCH, and CCC deformations. As can be seen from the B3LYP/6-311++G(d,p) scaled ab initio vibrational computations for the conformer A, CH3ab was located as pure mode or combined with CH2b from 1480 to 1445 cm^{-1} and observed from 1470 to 1450 cm^{-1}, while CH3sb appears essentially alone from 1390 to 1360 cm^{-1} and calculated in the same order of magnitude. HCC deformation DefCH of the tertiary carbon C4 appears alone for two modes calculated at 1351 and 1348 cm^{-1} and observed at 1350 cm^{-1} and contributes with CH2wa, CH2tw or CC stretching for two other modes calculated at 1299 to 1280 cm^{-1} and observed at the same frequencies.

Furthermore, the CC stretching acts within the range 1250–740 cm^{-1}, contributes essentially in combination with CH2ro, CH2tw, and CH3r, knowing that the most important modes involving predominately CC contributions were calculated at 1248 (40%), 896 (48%), 832 (55%), and 747 (74%) and observed at 1245, 897, 831, and 748 cm^{-1}, respectively. The latter band is very strong and polarized [49] in Raman spectrum as is assigned to total symmetric stretching (TS) of the tert-butyl group (60%) and C_2C_3 stretching (14%). Concerning the CCC deformation, it appears predominately in the 510–350 cm^{-1} interval or combined with CC torsions below 350 cm^{-1} knowing that the deformation mode of the central skeleton contributes predominately to $C_2C_3C_4$ (50%) and the two torsional modes involving predominately C_2C_3 and C_3C_4 torsions have the lowest frequencies of CCC deformation and CC torsion, respectively.

In order to complete our conformational analysis, the normal modes of secondary conformers based on the same B3LYP/6-311++G(d,p) scaled ab initio force field as the conformer A were determined. We noticed that all the observed frequencies were reproduced by the vibrational mode calculation of B, C, D, E, and F conformers, indicating once more, that all observed bands are common for the most stable conformers as well as the secondary ones.

Table 9 Local symmetry coordinates scale factors for DFT/B3LYP/6-311++G(d,p) of the most stable conformer A for 2,2,4-trimethyl pentane

Symmetry coordinates	B3LYP/6-311++G(d,p)
CCs	1.01301
CH3s	0.92422
CC3S	1.02364
CH2ss	0.92983
CHs	0.88961
CH3sb	0.94662
CH3ab	0.95051
CH3r	0.94198
CH2b	0.95913
CH2ro	0.94182
CH2wa	0.88360
CH2tw	0.97418
Def CH	0.99070
Def CCC	1.01094
CCtors	1.30289

Conclusions

In the light of this large theoretical and comparative study, we can conclude the following:

- A large exploration of the conformational space has led us to two very stable conformers and four other secondary ones, where the interaction between tert-butyl and isopropyl groups was a determining factor.
- All possible transitions between conformers are one-dimensional rotations around the C_3–C_4 bond and are confronted with isopropyl barriers to internal rotation.
- The B3LYP/6-311++G(d,p) optimization is slightly more stabilizing than MP2/6-311++G(d,p) and MP2/6-311++

Table 10 Observed and calculated B3LYP/6-311++G(d,p) vibrational frequencies (cm^{-1}) of 2,2,4-trimethylpentane

Mode nos	Experimental wavenumbers/cm^{-1}		Theoretical wavenumbers/cm^{-1}								PED (5%) with assignments
	FT-Raman	FT-IR	A	B	C	D	E	F	I°RA	I°IR	
1	2952	2956	2973	2974	2988	2988	2985	2985	44,90	25,36	C_6H3ds2(62)C_6H3ds1(31)
2	2952	2956	2964	2964	2969	2969	2973	2973	96,05	81,30	C_8H3ds2(69)−C_7H3ds2(14)−C_8H3ds1(8)−C_7H3ds1(5)
3	2952	2956	2960	2959	2956	2957	2963	2963	64,88	40,94	C_7H3ds2(55)C_8H3ds2(19)−C_1H3ds2(12)C_7H3ds1(9)
4	2952	2956	2958	2956	2955	2955	2958	2958	194,04	79,45	C_7H3ds1(29)C_1H3ds1(18)C_5H3ds1(17)C_8H3ds1(12)−C_5H3ds2(9)−C_7H3ds2(6)
5	2952	2956	2957	2955	2953	2953	2951	2951	31,74	87,80	C_5H3ds1(33)−C_5H3ds2(26)−C_8H3ds1(17)C_7H3ds2(11)−C_1H3ds1(10)
6	2952	2956	2956	2953	2951	2951	2948	2948	66,06	23,33	C_1H3ds2(66)−C_5H3ds1(9)C_7H3ds1(7)−C_8H3ds1(6)
7	2952	2956	2952	2949	2948	2948	2947	2947	93,84	46,45	C_5H3ds2(30)C_6H3ds1(30)C_5H3ds1(15)−C_6H3ds2(14)
8	2952	2956	2951	2948	2945	2945	2945	2944	15,04	0,74	C_8H3ds1(46)−C_7H3ds1(30)C_1H3ds2(11)
9	2952	2956	2950	2947	2944	2944	2943	2943	10,87	0,35	C_1H3ds1(68)−C_7H3ds1(16)−C_8H3ds1(8)
10	2952	2956	2946	2943	2942	2942	2941	2941	13,85	2,14	C_6H3ds1(33)−C_5H3ds2(27)−C_5H3ds1(23)−C_6H3ds2(15)
11	2933	2936	2930	2933	2934	2934	2932	2932	40,10	28,74	C_3H2as(95)
12	2904	2901	2903	2907	2907	2906	2908	2908	586,55	8,24	C_7H3ts(36)C_8H3ts(34)C_1H3ts(18)C_3H2ss(7)
13	2904	2901	2897	2898	2897	2897	2896	2896	125,98	49,69	C_6H3ts(60)C_5H3ts(21)−C_7H3ts(8)C_3H2ss(6)
14	2904	2901	2895	2894	2894	2894	2895	2895	33,30	28,91	C_8H3ts(54)−C_7H3ts(43)
15	2904	2901	2892	2892	2890	2890	2892	2892	75,42	34,83	C_1H3ts(71)−C_7H3ts(12)−C_8H3ts(8)
16	2904	2901	2891	2889	2887	2887	2890	2890	53,27	25,40	C_5H3ts(66)−C_6H3ts(24)
17	2868	2870	2885	2888	2886	2886	2884	2884	33,45	21,98	C_3H2ss(81)−C_5H3ts(8)−C_1H3ts(6)
18	2843	2845	2843	2844	2843	2843	2842	2842	20,13	18,24	C_4Hs(96)
19	*	1471	1482	1483	1485	1485	1486	1486	0,65	18,83	C_7H3ab2(24)C_1H3ab2(19)C_8H3ab1(17)C_8H3ab2(13)
20	1469	1471	1475	1476	1478	1478	1478	1478	1,21	0,73	C_3H2b(19)C_7H3ab1(19)C_6H3ab2(18)C_8H3ab2(14)C_5H3ab1(11)−C_8H3ab1(9)
21	1469	1471	1473	1474	1473	1473	1476	1475	2,06	14,37	C_7H3ab1(20)−C_6H3ab2(20)−C_1H3ab1(13)−C_5H3ab1(8)−C_7H3ab2(8)−C_5H3-ab2(7)−C3H2b(5)
22	1469	1471	1470	1471	1469	1469	1469	1469	1,99	11,34	C_1H3ab1(27)−C_8H3ab1(19)−C_6H3ab2(11)−C_5H3ab1(8)−C_1H3ab2(7)C_7H3a-b2(7)−C5H3ab2(6)
23	1469	1471	1467	1468	1468	1468	1464	1464	14,70	1,41	C_6H3ab1(33)C_5H3ab2(33)−C_5H3ab1(13)
24	1458	1459	1460	1461	1460	1460	1460	1459	1,92	3,73	C_6H3ab1(31)C_3H2b(16)C_5H3ab1(15)C_7H3ab2(7)−C_5H3ab2(7)C_8H3ab1(6)−-C8H3ab2(6)
25	1458	1459	1455	1456	1456	1456	1458	1457	14,15	1,18	C_3H2b(31)C_8H3ab1(17)−C_1H3ab2(15)−C_5H3ab1(11)−C_7H3ab1(6)
26	1458	1459	1453	1453	1451	1451	1452	1452	15,80	0,11	C_6H3ab2(29)−C_5H3ab1(22)−C_5H3ab2(20)C_7H3ab2(7)−C_1H3ab1(6)
27	1449	*	1449	1450	1448	1448	1445	1445	4,86	0,01	C_7H3ab2(33)−C_1H3ab1(12)−C_8H3ab2(12)−C_6H3ab1(9)C_5H3ab2(8)C_7H3a-b1(8)
28	1449	*	1446	1447	1447	1447	1444	1444	1,55	0,26	C_1H3ab2(25)C_3H2b(21)−C_8H3ab2(20)C_1H3ab1(12)−C_6H3ab1(8)
29	1449	*	1445	1446	1443	1443	1443	1443	0,66	0,27	C_7H3ab1(32)C_8H3ab1(16)C_1H3ab1(14)−C_8H3ab2(13)−C_1H3ab2(11)
30	*	1394	1393	1393	1390	1390	1393	1393	0,21	8,10	C_7H3sb(32)C_1H3sb(31)C_8H3sb(26)
31	1384	1384	1382	1384	1381	1381	1383	1384	0,27	3,01	C_6H3sb(45)C_5H3sb(44)
32	1361	1369	1366	1367	1370	1370	1368	1369	0,20	18,03	C_5H3sb(22)−C_6H3sb(21)C_7H3sb(19)
33	1361	1369	1365	1366	1363	1363	1366	1366	0,11	9,29	C_1H3sb(32)−C_7H3sb(23)−C_6H3sb(12)C_5H3sb(11)
34	1361	1369	1363	1365	1362	1362	1360	1361	0,42	1,89	C_8H3sb(50)−C_1H3sb(15)−C_7H3sb(8)
35	1350	1350	1351	1353	1356	1356	1352	1352	3,55	4,53	DefC$_4$H(37)Def'C$_4$H(9)

Table 10 (continued)

Mode nos	Experimental wavenumbers/cm^{-1}		Theoretical wavenumbers/cm^{-1}								PED (5%) with assignments
	FT-Raman	FT-IR	A	B	C	D	E	F	I°RA	I°IR	
36	1350	1350	1348	1349	1348	1348	1346	1346	1,96	0,70	Def'C_4H(33)−DefC_4H(15)
37	1299	*	1299	1301	1300	1301	1302	1301	3,25	0,85	C_3H2tw(30)−Def'C_4H(20)CC3DS2(10)
38	1281	1283	1280	1281	1280	1280	1285	1284	6,40	2,30	C_3H2wa(42)DefC_4H(11)CC3DS(18)
39	1245	1254	1248	1250	1249	1249	1249	1249	8,35	6,93	C_2C_3s(24)SD(16)−C_1H3r1(11)
40	1204	1206	1210	1209	1208	1208	1212	1213	5,85	4,20	CC3DS1(16)−C_3H2wa(13)C_7H3r2(10)
41	1204	1206	1205	1204	1206	1205	1199	1199	2,58	3,65	C_3H2tw(13)−CC3DS2(13)
42	1166	1172	1169	1168	1172	1172	1188	1188	2,93	6,29	C_3C_4s(18)−C_6H3r2(13)C_5H3r2(10)−C_5H3r1(10)−C_4C_5s(7)−C_4C_6s(7)
43	1109	*	1118	1117	1117	1117	1100	1099	1,70	0,62	C_5H3r1(12)−C_3C_4s(12)−C_4C_5s(9)−C_6H3r2(8)−C_5H3r2(6)−C_7H3r2(5)
44	1097	*	1098	1098	1097	1097	1080	1080	4,73	0,50	C_3H2tw(16)−C_4C_6s(11)C_1H3r2(11)C_6H3r1(10)C_4C_5s(9)
45	*	*	1015	1015	1017	1017	1013	1013	1,20	0,03	C_8H3r1(32)−C_1H3r1(12)−C_7H3r2(7)C_1H3r2(6)−C_7H3r1(5)
46	1016	1015	1008	1007	1005	1005	1012	1011	1,13	0,14	C_7H3r1(30)−C_1H3r1(23)C_8H3r2(8)
47	977	979	976	975	975	975	981	980	2,01	2,48	C_3C_4s(30)−C_2C_3s(15)C_6H3r1(13)C_5H3r1(10)−C_4C_6s(7)
48	951	*	947	946	947	947	950	950	3,75	0,04	C_6H3r1(32)−C_5H3r1(30)−C_4C_5s(17)C_4C_6s(13)
49	951	*	929	929	930	930	934	934	0,09	0,02	C_1H3r2(37)C_7H3r2(28)C_8H3r2(28)
50	926	929	925	925	924	924	929	929	3,35	0,34	C_7H3r2(18)−CC3DS2(18)C_8H3r1(16)−CC3DS1(15)−C_1H3r1(11)−C_1H3r2(7)
51	926	929	921	920	921	921	924	924	7,43	0,82	CC3DS1(22)C_8H3r2(22)−C_7H3r1(17)−CC3DS2(17)C_1H3r1(10)
52	926	929	907	907	908	908	904	903	3,14	0,46	C_5H3r2(37)C_6H3r2(32)Def'C_4H(11)
53	897	*	896	896	898	899	899	899	7,62	0,13	C_2C_3s(25)−CC3TS(13)−C_4C_5s(11)−C_4C_6s(9)C_6H3r2(8)C_7H3r1(6)C_8H3r1(6)-C1H3r1(5)
54	858	*	857	859	859	860	857	857	2,42	0,60	C_3H2ro(48)−CC3DS(29)−C_4C_5s(5)
55	824	*	832	831	819	819	811	810	5,52	0,61	C_4C_6s(23)C_3C_4s(16)C_4C_5s(10)−CC3TS(6)
56	743	*	748	747	750	750	726	726	12,05	0,19	CC3TS(60)C_2C_3s(14)
57	506	510	506	504	517	517	570	572	4,66	0,03	SD(30)$C_2C_3C_4$b(15)$C_4C_5C_6$b(11)$C_3C_4C_5$b(6)
58	456	453	456	456	453	453	416	418	0,38	0,33	$C_3C_4C_6$b(26)−R1(20)$C_3C_4C_5$b(15)−AD2(6)
59	417	415	417	418	425	425	401	403	0,34	0,10	$C_4C_5C_6$b(20)−R2(13)−SD(12)−AD(18)−$C_3C_4C_6$b(6)
60	*	*	409	408	418	418	392	394	0,40	0,05	$C_4C_5C_6$b(26)R2(14)−AD2(13)AD1(13)−SD(10)
61	*	*	386	385	374	373	363	365	0,12	0,02	AD1(39)$C_3C_4C_6$b(23)−$C_3C_4C_5$b(6)
62	356	356	361	359	356	356	359	361	0,55	0,05	AD2(39)$C_3C_4C_5$b(15)−C_4C_5tr(10)−SD(7)
63	322	*	326	334	340	340	344	343	1,23	0,00	C_2C_8tr(65)−C_1C_2tr(16)
64	322	*	317	311	320	320	327	326	0,98	0,02	C_2C_7tr(45)−C_1C_2tr(33)
65	300	*	307	308	303	303	313	312	0,26	0,05	C_4C_5tr(22)AD2(16)R2(16)−R1(12)−C_2C_8tr(10)−C_4C_6tr(9)
66	300	*	289	284	295	295	284	283	0,52	0,05	C_4C_5tr(26)−R2(18)$C_3C_4C_5$b(17)−C_1C_2tr(9)AD1(5)
67	*	*	285	281	274	274	269	269	0,23	0,01	R2(17)−$C_4C_5C_6$b(15)$C_3C_4C_6$b(13)−AD1(9)−C_4C_6tr(6)R1(5)−SD(5)
68	267	*	272	263	270	270	258	258	0,05	0,00	C_4C_6tr(62)C_4C_5tr(27)
69	*	*	254	251	250	250	253	254	0,03	0,01	C_2C_7tr(39)C_1C_2tr(32)C_2C_8tr(20)
70	197	*	189	189	187	186	201	202	0,16	0,02	$C_2C_3C_4$b(50)−R1(24)−$C_3C_4C_5$b(11)
71	*	*	102	110	129	129	144	144	0,03	0,00	C_2C_3tr(69)−C_3C_4tr(13)
72	*	*	59	63	38	39	58	58	0,17	0,00	C_3C_4tr(71)

G(d,p) rotational barriers, and their corresponding inversion barriers between secondary conformers are larger than that of B3LYP/6-311++G(d,p).

- The secondary conformers E and F are slightly softer, and thus more reactive than the other forms, while the electrostatic molecular potential is almost identical for all conformers.
- According to E(2) values, the conformational flexibility influences intramolecular charge transfers of natural bond orbitals and the larger values of E(2) are explained with the σ_{CH}–σ^*_{CC} interactions.
- The magnitude of the first-order hyperpolarizability is found to be very sensitive to conformational behavior, contrary to mean polarizability and the anisotropy of the polarizability. However, the title molecule has only moderate nonlinear optics activity.
- The theoretical relative ^{13}C and ^{1}H-NMR chemical shift predictions confirmed their conformational sensitivity, by their compatibility with natural NPA charges. In addition, their confrontation in the experiment confirms that the conformers E and F are not only of lower stability but also require a relatively high barrier of rotation.
- Only the least stable secondary conformers E and F are easily distinguishable from the other conformers by TD-DFT calculations on electronic absorption spectra and the use of DMSO solvent has a noticeable effect on oscillator strengths, which increase by about 20 to 25% for all the conformers.
- Spectral temperature sensitivity and scaled vibrational assignment for the six lowest conformers A–F are in a good agreement, as both procedures eliminate any possibility of conformational exchange between conformers.
- The computed scaled frequencies are well predicted as they are in a good agreement with the experimental data rms deviation, not exceeding 10 cm^{-1} for all frequencies and 6 cm^{-1} for frequencies below 1500 cm^{-1}.

As a perspective of this work, we plan to extend our study to comparable molecules, especially the other molecules in the trimethylpentane series, with more advanced quantum methods.

References

1. Dabelstein W, Reglitzky A, Schutze A, Reders K (2012) Automotive fuels. In: Ullmann's encyclopedia of industrial chemistry. Wiely-VCH, Weinheim, pp 426–457
2. Frédéric B (2006) Mécanismes cinétiques pour l'amélioration de la sécurité des procédés d'oxydation des hydrocarbures. Dissertation, University of Nancy
3. Chiari L et al (2014) Cross sections for positron impact with 2,2,4-trimethylpentane. J Phys Chem A 118:6466–6472
4. National Center for Biotechnology Information (2018) 2,2,4-Trimethyl pentane – compound summary. PubChem Compound Database. CID=10907, https://pubchem.ncbi.nlm.nih.gov/compound/10907. Accessed 2 March 2018
5. Enech OC (2011) A review on petroleum: source, uses, processing, products and the environement. J Appl Sci 11(12):2084–2091
6. Suvitha A, Periandy S, Govindarajan M, Gayathri P (2014) Vibrational analysis using FT-IR, FT-Raman spectra and HF - DFT methods and NBO, NLO, NMR, HOMO-LUMO, UV and electronic transitions studies on 2,2,4 trimethyl pentane. Spectrochim Acta A Mol Biomol Spectrosc 138:900–912
7. U.S. Environmental Protection Agency (1999) Integrated Risk Information System (IRIS) on 2,2,4-trimethyl pentane. National Center for Environmental Assessment, Office of Research and Development, Washington, DC
8. Guntram R, Peter P (1995) Transferable scaling factors for density functional derived vibrational force fields. J Phys Chem 99:3093–3100
9. Cox SR, Williams DE (1981) Representation of the molecular electrostatic potential by a net atomic charge model. J Comput Chem 2(3):304–323
10. Reed AE, Weinhold F (1983) Natural bond orbital analysis of near-Hartree–Fock water dimer. J Chem Phys 78(6):4066–4073
11. Keeler J (2011) Understanding NMR spectroscopy. Wiley, New York
12. Owen AE (1996) Fundamentals of UV-visible spectroscopy. Hewlett-Packard Company, Palo Alto
13. Mouatarif S, Aboulmouhajir A (2004) An ab initio and DFT study of the conformational stability in branched alkanes: illustration for 3 , 3-dimethylhexane. J Mol Struct 709:157–161
14. Werner HJ, Knowles PJ, Knizia G, Manby FR, Schütz M (2012) Molpro: a general-purpose quantum chemistry program package. WIREs Comput Mol Sci 2:242–253
15. The Magrid Virtual Organization of the Moroccan Grid Infrastructure (2016) CNRST/MAGRID. http://www.magrid.ma. Accessed 20 Apr 2016
16. Ayala PY, Scuseria GE (1999) Linear scaling second-order Moller–Plesset theory in the atomic orbital basis for large molecular systems. J Chem Phys 110:3660–3671
17. Lee C, Yang W, Parr RG (1988) Development of the Colle-Salvetti correlation-energy formula into a functional of the electron density. Phys Rev B 37:785–789
18. Krishnan R et al (1980) Self-consistent molecular orbital methods. XX. A basis set for correlated wave functions. J Chem Phys 72: 650–654
19. Mouatarif S, Van Alsenoy C, Aboulmouhajir A (2008) Conformational dependence of vibrational spectra in some branched octanes: 3,3- and 2,2-dimethylhexanes. Spectrosc Lett 41:87–99
20. Zhurko G, Zhurko D (2017) ChemCraft, version 1.8. http://www.chemcraftprog.com. Accessed 04 May 2018
21. Frisch MJ, Trucks GW, Schlegel HB, Scuseria GE, Robb MA, Cheeseman JR, Scalmani G, Barone V, Mennucci B, Petersson GA, Nakatsuji H, Caricato M, Li X, Hratchian HP, Izmaylov AF, Bloino J, Zheng G, Sonnenberg JL, Hada M, Ehara M, Toyota K, Fukuda R, Hasegawa J, Ishida M, Nakajima T, Honda Y, Kitao O, Nakai H, Vreven T, Montgomery Jr JA, Peralta JE, Ogliaro F, Bearpark M, Heyd JJ, Brothers E, Kudin KN, Staroverov VN, Keith T, Kobayashi R, Normand J, Raghavachari K, Rendell A, Burant JC, Iyengar SS, Tomasi J, Cossi M, Rega N, Millam JM, Klene M, Knox JE, Cross JB, Bakken V, Adamo C, Jaramillo J, Gomperts R, Stratmann RE, Yazyev O, Austin AJ, Cammi R, Pomelli C, Ochterski JW, Martin RL, Morokuma K, Zakrzewski VG, Voth GA, Salvador P, Dannenberg JJ, Dapprich S, Daniels AD, Farkas

O, Foresman JB, Ortiz JV, Cioslowski J, Fox DJ (2010) Gaussian 09, revision B.01. Gaussian, Inc., Wallingford
22. Alecu IM, Zheng J, Zhao Y, Truhlar DG (2010) Computational thermochemistry: scale factor databases and scale factors for vibrational frequencies obtained from electronic model chemistries. J Chem Theory Comput 6:2872–2887
23. Martin JML, Van Alsenoy C (2007) GAR2PED, a program to obtain a potential energy distribution from a Gaussian archive record. University of Antwerp, Antwerp
24. Keresztury G et al (1993) Vibrational spectra of monothiocarbamates-II. IR and Raman spectra, vibrational assignment, conformational analysis and ab initio calculations of S-methyl-N,N-dimethylthiocarbamate. Spectrochim Acta A Mol Biomol Spectrosc 49:2019–2026
25. Keresztury G, Chalmers JM, Griffith PR (2002) Raman spectroscopy: theory. Hand book of vibrational spectroscopy. Wiley, New York
26. Grabowski ZR, Rotkiewicz K, Rettig W (2003) Structural changes accompanying intramolecular electron transfer: focus on twisted intramolecular charge-transfer states and structures. Chem Rev 103:3899–4032
27. Vijayachamundeeswari SP, Yagna Narayana B, Jone Pradeepa S, Sundaraganesan N (2015) Vibrational analysis, NBO analysis, NMR, UV-VIS, hyperpolarizability analysis of Trimethadione by density functional theory. J Mol Struct 1099:633–643
28. Reed AE, Curtiss LA, Weinhold F (1988) Intermolecular interactions from a natural bond orbital, donor-acceptor viewpoint. Chem Rev 88:899–926
29. Natarajan S, Shanmugam G, Dhas SAMB (2008) Growth and characterization of a new semi organic NLO material: L-tyrosine hydrochloride. Cryst Res Technol 43:561–564
30. Avci D (2011) Second and third-order nonlinear optical properties and molecular parameters of azo chromophores: semiempirical analysis. Spectrochim Acta A Mol Biomol Spectrosc 82:37–43
31. Avci D, Basoglu A, Atalay Y (2010) Ab initio HF and DFT calculations on an organic non-linear optical material. Struct Chem 21: 213–219
32. Altürk S, Avcı D, Tamer Ö, Atalay Y (2017) Comparison of different hybrid DFT methods on structural, spectroscopic, electronic and NLO parameters for a potential NLO material. Comput Theor Chem 1100:34–45
33. Colherinhas G, Fileti EE, Malaspina T (2018). J Mol Model 24:181. https://doi.org/10.1007/s00894-018-3719-3
34. Iozzi MF, Mennucci B, Tomasi J, Cammi R (2004) Excitation energy transfer (EET) between molecules in condensed matter: a novel application of the polarizable continuum model (PCM). J Chem Phys 120:7029–7040. https://doi.org/10.1063/1.1669389
35. Guelai A, Brahim H, Guendouzi A et al (2018) Structure, electronic properties , and NBO and TD-DFT analyses of nickel (II), zinc (II), and palladium (II) complexes based on Schiff-base ligands. J Mol Model 24:301. https://doi.org/10.1007/s00894-018-3839-9
36. Marques MAL, Gross EKU (2003) Time-dependent density functional theory. In: Fiolhais C, Nogueira F, Marques MAL (eds) A primer in density functional theory. Lecture notes in physics, vol 620. Springer, Berlin
37. Pauzat F, Talbi D, Miller M, Defrees D, Ellinger Y (1992) Theoretical IR spectra of ionized naphthalene. J Phys Chem 96: 7882–7886
38. Lide Jr DR, Mann DE (1958) Microwave spectra of molecules exhibiting internal rotation. IV. Isobutane, tertiary butyl fluoride, and trimethylphospine. J Chem Phys 29:914. https://doi.org/10.1063/1.1744611
39. Pitzer KS, Kilpatrick JE (1946) The entropies and related properties of branched paraffin hydrocarbons. Chem Rev 393:435–447. https://doi.org/10.1021/cr60124a005
40. Jha O, Yadav TK, Yadav RA (2017) Comparative structural and vibrational study of the four lowest energy conformers of serotonin. Spectrochim Acta A Mol Biomol Spectrosc 173:307–317
41. Shankar Rao YB, Prasad MVS, Udaya Sri N, Veeraiah V (2016) Vibrational (FT-IR, FT-Raman) and UV-visible spectroscopic studies, HOMO-LUMO, NBO, NLO and MEP analysis of benzyl (imino (1H-pyrazol-1-yl) methyl) carbamate using DFT calculaions. J Mol Struct 1108:567–582
42. Sasikala V, Sajan D, Chaitanya K, Sundius T, Devi TU (2017) Qualitative and quantitative approach towards the molecular understanding of structural, vibrational and optical features of urea ninhydrin monohydrate. Mater Chem Phys 191:20–34
43. Sun YX et al (2009) Experimental and density functional studies on 4-(3,4-dihydroxybenzylideneamino)antipyrine, and 4-(2,3,4-trihydroxybenzylideneamino)antipyrine. J Mol Struct THEOCHEM 904:74–82
44. National Institute of Advanced Industrial Science and Technology (AIST) (1999) https://sdbs.db.aist.go.jp/sdbs/cgi-bin/direct_frame_disp.cgi?sdbsno=2353&spectrum_type=CNMR&fname=CDS00677. Accessed 16 April 2019
45. National Institute of Advanced Industrial Science and Technology (AIST) (1999) https://sdbs.db.aist.go.jp/sdbs/cgi-bin/direct_frame_disp.cgi?sdbsno=2353&spectrum_type=HNMR&fname=HSP03717. Accessed 16 April 2019
46. Condon E (1947) The Franck-Condon principle and related topics. Am J Phys 15:365–374. https://doi.org/10.1119/1.1990977
47. Aboulmouhajir A, Mouatarif S et al (2017) Theoretical and spectroscopic investigations of conformations, rotational barriers and scaled vibrations of 2 , 3-dimethyl hexane. Mediterr J Chem 6: 60–70
48. Mirkin NG, Krimm S (2000) Ab initio analysis of the vibrational spectra of conformers of some branched alkanes. J Mol Struct 550–551:67–91
49. Gough KM, Lupinetti C, Dawes R (2004) Computation and interpretation of Raman scattering intensities. J Comput Methods Sci Eng 4:597–609